RSC Advances

ROYAL SOCIETY OF CHEMISTRY

www.rsc.org/advances

Graphical abstract

PdCoP alloy nanoparticle networks prepared using inert bubbles as template exhibited high activity for hydrazine oxidation.

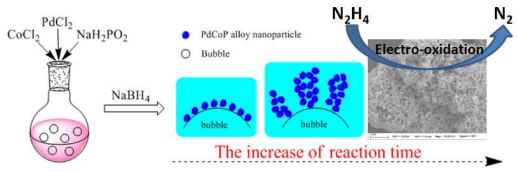

Journal Name

RSCPublishing

ARTICLE

Room-temperature synthesis with inert bubble templates to produce "clean" PdCoP alloy nanoparticle networks for enhanced hydrazine electro-oxidation

Cite this: DOI: 10.1039/xoxxoooooox

Received ooth January 2012,
Accepted ooth January 2012

DOI: 10.1039/xoxxoooooox

www.rsc.org/

Yuanyuan Ma,[a] Rongfang Wang,[a*] Hui Wang,[a] Julian Key[b] and Shan Ji[b**]

PdCoP alloy nanoparticle networks (ANN) were prepared by simultaneous reduction of $PdCl_2$, $CoCl_2$ and NaH_2PO_2 with $NaBH_4$ using N_2 bubbles as soft-templates at room temperature. The PdCoP ANN porous structure was formed at the inert gas bubble surface, and could be obtained with varying ratios of precursors to produce catalysts with different compositions and catalytic activity. PdCoP ANN produced markedly higher hydrazine oxidation activity than PdCo ANN and PdCoP grain aggregates, and catalytic activity varied with different ratios of Pd, Co and P. We conclude that PdCoP ANN are promising hydrazine oxidation catalysts and that the developed method provides a facile and convenient mean of producing mesoporous catalysts with high-surface area.

1. Introduction

Direct hydrazine fuel cells (DHFCs) are attractive candidate power sources for both portable power applications and electric vehicles. Compared to other types of fuel cells, DHFC's have the following virtues: (i) their open-circuit cell voltage of 1.61 V is higher than that of formic acid and direct methanol fuel cells; (ii) they produce higher energy and power density than the hydrogen fuel cell (5400 W h L^{-1}); and (iii) the products of hydrazine oxidation (N_2 and H_2O) are neither harmful to the environment nor carbon-containing[1]. Over the past few decades, noble-metals such as Pt[2,3], Pd[4,5], and Au[6], have received much attention as hydrazine electrooxidation catalysts. However, like many other types of fuel cells, the high cost of noble metals hinders the commercial success of DHFC's. Development of lower cost and highly efficient electrocatalysts for electro-oxidation of hydrazine therefore remains a key research goal.

Bimetallic and multimetallic alloy catalysts (compared to catalysts comprising a single noble metal element) have been shown to produce higher catalytic activity due to synergistic effect between their different components[7-10]. Various factors such as morphology, composition, and nano-structural architecture can be modified to improve the catalytic performance of metal-based alloys[11]. In particular, three-dimensional porous or network-like structures are of great interest due to their high surface area-to-volume ratio, low density, high gas permeability (compared to their solid counterparts), and high density of atomic scale defects[12]. Such structures are often synthesized using hard templates or chemical/electrochemical dealloying from a binary or multicomponent alloy[13-15]. However, these methods are rather uneconomical for mass production due to their sacrificial components. Recently, Zhang's group synthesized a series of noble alloy networks, including PtNi[16], PtCo[17] and PdP[18] alloy networks, by reducing metal precursors with $NaBH_4$ in water using different soft surfactant templates. The resultant catalysts had high catalytic activity for either oxidation of methanol or formic acid, as well as for the oxygen reduction reaction. However, reports also showed that effective removal of adsorbed surfactant from the surface of metals or alloys, to obtain a "clean" surface, was a difficult process[19]. At the same time, the sol−gel approach without the help of templates has the potential for the formation of porous structures to overcome the above-mentioned drawbacks. Herrmann et al. prepared a series of Pd-based alloys by the sol-gel approach using supercritical drying[20]; however, the process is neither economical nor simple. Meanwhile, Lu et al. prepared PdCoP alloy networks by reducing $K_2PdCl_4/K_3Co(CN)_6$ cyanogel without any surfactants [21], but the precursor, $K_3Co(CN)_6$, is strongly toxic. Therefore, the search for a facile, green, low-cost and universal synthetic processes for making "clean" surface, porous or network-like nanomaterials appears to remain challenging.

The use of gas bubbles as soft template, developed by Li's group, offers a novel, simple and effective approach. In this method, gas-liquid interface can be acted as the agglomeration/nucleation center of the nanocrystals with special morphology[22]. In general methods, the surfactants and

capping agents were introduced to act as templates for special shape, but these reagents are hard to completely remove from the final products in the case of maintaining the morphology of the products[23]. The presence of capping agents around the products may severely limit their chemical activity[24]. That gas bubbles serve as templates avoiding the introduction of surfactant or capping agents e.g. impurities. Li's group used gas bubbles generated during the reaction process as a template to prepare CoTe and NiTe nanocluster wires[25] and ZnSe hollow microspheres. In our previous work, we introduced inert bubbles, which directly served a similar role. In the present work, we have extended this green and facile synthesis method to prepare PdCoP alloy nanoparticle networks (ANN) as catalysts for hydrazine oxidation, without the use of a strongly toxic precursor. We report PdCoP ANN prepared by a one-step co-reduction of metal precursors using N_2 bubbles as template, and show the composition of the PdCoP alloys can be modulated by adjusting the initial molar ratio of the metal precursors, while preserving the unique network structure. The method offers a mean for developing highly efficient catalysts with optimal chemical composition.

2. Experimental

2.1 Synthesis

All reagents were of analytic grade and ultrapure water was used throughout the experiments. To prepare PdCoP nanoparticle alloy networks with a molar ratio of Pd:Co:P=1:10:14, we first made three solutions as described in our previous work[26] : (1) 270 mg of $CoCl_2 \cdot 6H_2O$ and 160 mg of $NaH_2PO_2 \cdot H_2O$ were dissolved in 30 mL water bubbled continuously with N_2, (2) 80.6 mg of $NaBH_4$ was dissolved in 20 mL water and the solution was transferred to a constant funnel, and (3) 20 mg of $PdCl_2$ was dissolved in 10 mL water and adjusted to pH ~ 9 using 6 mol L^{-1} NaOH solution with vigorous stirring. Solution (2) was added drop-wise into solution (1) under the stirring conditions and bubbled with N_2. Then, solution (3) was rapidly added to the mixture and stirred vigorously for another 4 h with continuously bubbled N_2. In the reaction scheme, $PdCl_2$, $CoCl_2$, and $NaH_2PO_2 \cdot H_2O$ were reduced to produce PdCoP and $NaBH_4$ via the following reactions:

$$Pd^{2+} \xrightarrow{NaBH_4} Pd$$

$$Co^{2+} \xrightarrow{NaBH_4} Co$$

$$H_2PO_2^- \xrightarrow{NaBH_4} P+H_2O$$

$$xPd+yCo+zP \longrightarrow Pd_xCo_yP_z$$

The resultant precipitate was collected by filtration, washed with 6 mol L^{-1} ammonia solution, then washed with deionized water several times and stored in ethanol solution. To obtain alloy networks of different composition, we altered the precursor ratio as listed below in Table S1.

2.2 Characterization

XRD patterns were recorded on a Shimadzu XD–3A (Japan) using filtered Cu-K_α radiation (λ = 0.15418 nm) generated at 40 kV and 30 mA. Scans for 2θ values were recorded at 4° min^{-1}. Scanning electron microscopy (SEM) images were obtained using a Carl Zeiss Ultra Plus. Transmission electron micrographs (TEM), high angle annular dark field scanning transmission electron microscopy (HAADF-STEM) images of the catalysts were taken on a JEOL (JEM-2000 FX) microscope operating at 200 kV. The specific surface area was determined using the Brunauer-Emmett-Teller (BET) method and the density functional theory (DFT) method was used to analyze the full range of the pore size distribution. The average chemical compositions of the catalysts were obtained using an IRIS advantage inductively coupled plasma atomic emission spectroscopy (ICP-AES) system (Thermo, America). X-ray photoelectron spectra (XPS) was acquired with a VG Escalab210 spectrometer fitted with Mg 300 W X-ray source.

2.3 Electrochemical measurements

Electrochemical measurements were carried out using an electrochemical work station (CHI 650D). A common three-electrode electrochemical cell was used for the measurements. The counter and reference electrodes were a platinum wire and an Ag/AgCl (3 mol L^{-1} KCl) electrode respectively. The working electrode was prepared on a 5-mm diameter glassy carbon disk, 2 mg of catalyst was dispersed ultrasonically in 0.4 mL Nafion/ethanol (0.25% Nafion) solution, and 16 μL was pipetted and dried in air on the surface of glassy carbon.

3. Results and discussion

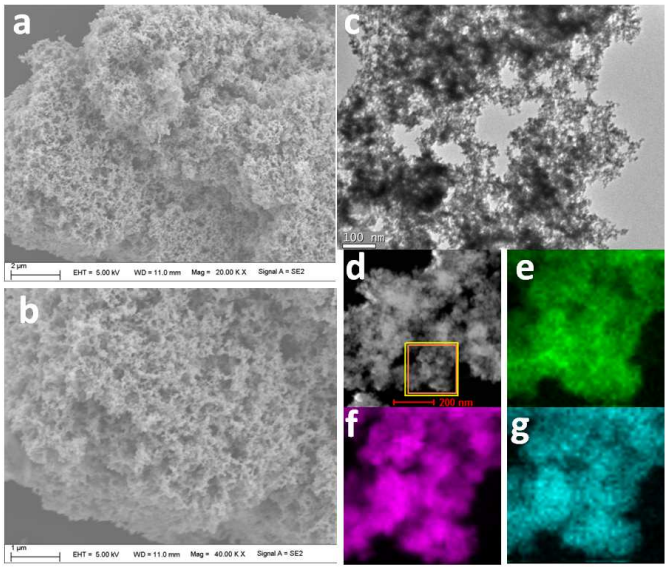

Fig. 1 (a,b) SEM images at different magnifications, (c) TEM image, (d) HAADF-STEM image, and the elemental mapping of Pd (e), Co (f), and P (g) of PdCoP-3.

PdCoP ANN (alloy nanoparticle networks) were prepared by co-reduction of $PdCl_2$, $CoCl_2$, and NaH_2PO_2 in the presence of $NaBH_4$ as a reducing agent and N_2 bubbles as a template at room temperature (see ESI† for details). Low magnification scanning electron microscopy (SEM) (Figure 1a) showed the

PdCoP-3 comprised an extensive network-like structure on a large scale. High magnification (Figure 1b) showed that the network-like structure was constructed from sub-10 nm aligned nanoparticles, which were also visible using Transmission electron micrographs (TEM) (Figure 1c). High resolution TEM displayed in Figure S1(ESI†) presented clear lattice planes, indicating PdCoP-3 possessed a crystalline structure. The chemical microstructure of PdCoP-3 nanoparticles was examined using electron energy loss spectroscopic mapping. Figure 1d shows the high angle annular dark field scanning transmission electron microscopy image of PdCoP-3 where the area circled by the orange box was spectroscopically imaged. Figure 1e–g shows the distribution of Pd, Co and P elements in PdCoP-3 respectively. Overlapping positions of the Pd (green) Co (purple), and P (blue) distributions indicates formation of PdCoP alloy structure. Using ICP analysis (ESI†, Table S1) the atomic ratio of Pd:Co:P in the bulk composition of PdCoP-3 was 1:5.6:11.

It is well established that the activity of multimetallic alloy electrocatalysts can vary according to their compositional ratio of elements. Therefore, synthesis of PdCoP ANN samples with varying ratios of elemental composition, while preserving the same morphology, would allow a further mean of optimizing PdCoP ANN catalytic activity. To obtain variations in PdCoP ANN composition, we adjusted the molar ratio of $PdCl_2/CoCl_2$ precursors from 1/6, 1/8, 1/12, to 1/14. Figure S2 (see ESI†) shows PdCoP ANN samples with different compositions shared similar network-like structure with nanoparticle frameworks between 5–9 nm in diameter. The actual Pd/Co/P atomic ratios were determined by ICP (listed in Table S1), and were close to the initial ratios of their reactant precursors.

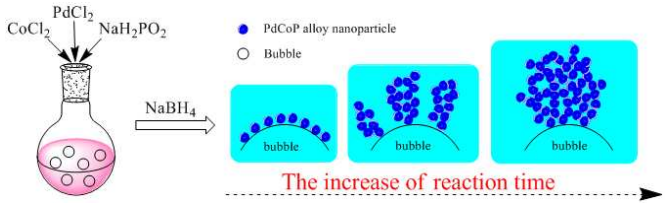

Scheme 1. Schematic process of PdCoP ANN formation on inert gas bubbles.

To elucidate the role of N_2 gas bubbles in the formation of porous structure, a series of control experiments was carried out during PdCoP ANN preparation. Firstly, to demonstrate the importance of the bubbles in network formation, synthesis in the absence of N_2 bubbles produced PdCoP grain aggregates (PdCoP GA) instead of a network structure (ESI,† Figure S3). Secondly, to determine if any specific chemical affinity to N_2 gas played a role in forming network structure, synthesis was carried out using two other inert gasses, argon and helium. Figure S4 shows that all three gasses produced no obvious difference in network structure. Thirdly, Time-dependent experiments was carried out and shown in Figure S5. We found that a reaction time 0.5 h produced many aggregate clusters consisting of small nanoparticles (ESI,† Figure S5a), whereas a 1.5 h reaction time produced the extensive network structure (ESI,† Figure S5b). Therefore, we hypothesize, according to our previously proposed N_2 bubble soft-template model[26], that the formed PdNiP particles aggregate at the interface between the bubble and aqueous solution. With increased reaction time, sufficiently high aggregation produces the network structure

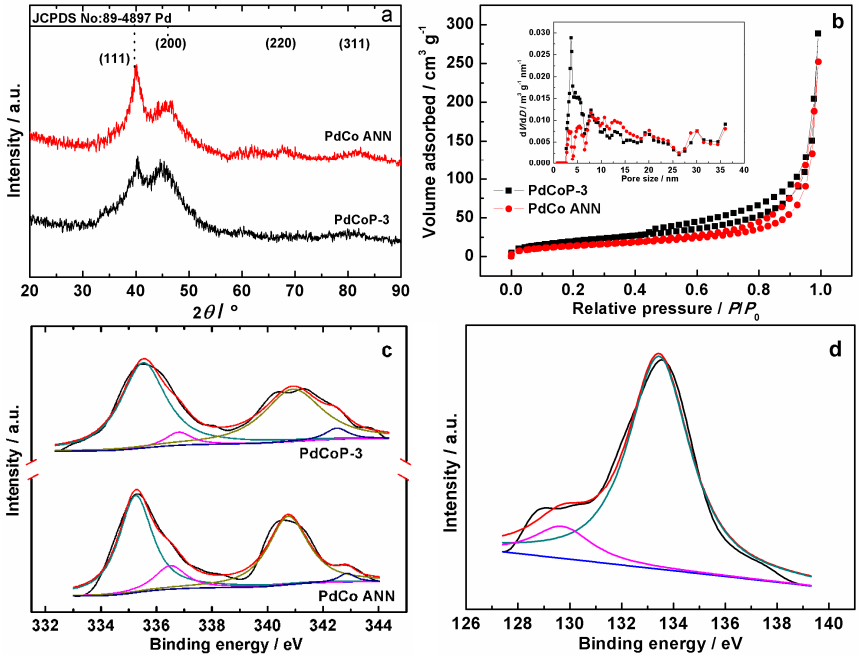

Fig. 2 (a) XRD patterns, (b) Nitrogen isotherms and (Inset) the corresponding pore size distribution of PdCoP-3 and PdCo ANN. (c) Pd 3d of PdCoP-3 and PdCo ANN. (d) P 2p XPS spectrum of PdCoP-3.

Journal Name RSCPublishing

ARTICLE

(Scheme 1). In addition, we successfully extending the method to synthesis of PdCo alloy nanoparticle networks (PdCo ANN) (ESI,† Figure S6).

Here, it is beneficial to do the comparison between the bubble-templates synthesis and solvothermal synthesis since solvothermal synthesis with surfactants is a widely used technique. We prepared PdCoP samples by solvothermal method, and their SEM images were present in Figure S7 (ESI† Table S2). We used water and ethanol as solvent and CTAB and SDS as surfacetants, respectively. Among four samples, only one sample prepared using ethanol as slovent and CTAB as surfactant presented network structure. However, there is a few big particles in the sample. Based on the above facts, the bubble-templates synthesis is a facile method to form network structure.

Phase analysis of PdCoP ANN with various compositions was carried out using XRD. PdCoP-3 and PdCo ANN (Figure 2a) produced diffraction peaks at around 40, 46, 68, and 82° corresponding to (111), (200), (220), and (311) diffractions respectively, which fit the typical pattern of polycrystalline Pd face-centered cubic (fcc) phase (JCPDS 89-4897: marked with the dot black vertical lines). The diffraction peaks of PdCoP-3 and PdCo ANN shifted to a slightly higher 2θ degree compared to pure Pd, implying that the lattice parameter had shrunk because Pd atoms were replaced by smaller atoms. The peaks of PdCoP-3 had a slightly positive shift compared to PdCo ANN, indicating a shrinkage of the Pd lattice in PdCoP-3 compared to pure PdCo perhaps due to replacement of Pd atoms by P atoms. In addition, upon the increasing content of Co in PdCoP ANN, the diffraction peaks in Figure S8 (ESI,†) shifted towards high 2θ angle from PdCoP-1 to PdCoP-4, indicating that the lattice parameter became smaller with the increasing amount of Co atoms inserted into the Pd lattice.

The porosity and the surface area of PdCoP ANN were evaluated by nitrogen physisorption. High surface areas for the PdCoP ANN samples were expected owing to their network-like structure. Figure 2b shows N_2 adsorption-desorption isotherms for PdCoP-3 and PdCo ANN. Figure 4 shows a hybrid II/IVisotherm (according to IUPAC classification) was predominant, indicating multilayer adsorption behavior, and the absence of a plateau for high relative pressure values revealed the presence of large mesopores and macropores inside the material[27]. The insets of Figure 2b show the corresponding cumulative pore volumes calculated by applying DFT (density functional theory). In the evaluated range between ca. 0.8 and 36 nm, the distribution was broad in the mesopore range, did not reach a plateau, and no prevalent pore size was observed. This correlates to the SEM characterization of open pores and tunnels. This hierarchical pore system should greatly favor the transport of reactants and reactant products to and from the catalyst surface respectively. Based on the N_2 sorption data, the BET surface area and total pore volume of PdCoP-3 were 73.1 $m^2\ g^{-1}$ and 0.446 $cm^3\ g^{-1}$ respectively, and were higher than those of PdCo at 49.5 $m^2\ g^{-1}$ and 0.390 $cm^3\ g^{-1}$ respectively. The result could relate to the addition of P which reduces the particle size[18]. PdCoP-3 also had a large the surface area and pore volume than PdCoP GA (ESI,† Figure S9 and Table S3), suggesting that the network-like structure would provide a larger surface area for catalysis than solid particle aggregated structure. In addition, the surface area of PdCoP ANNs did not change in a regular way with the molar ratio of PdCo, suggesting that multiple factors affect the surface area, which should be further studied in future.

The surface composition and the chemical state of the elements in PdCoP-3 and PdCo ANN were analyzed by XPS. In the Pd 3d spectrum of two samples (Figure 2c), the Pd 3d signals fitted into two pairs of doublets with a spin–orbit separation of 5.4 eV, which corresponded to Pd(0) and Pd(II) respectively. The binding energy (BE) and the composition are listed in Table S4 (ESI†). Pd in the two samples existed predominately in the oxidized state, and the percentage of Pd(0) in PdCoP-3 was higher than that in PdCo ANN. The BEs of Pd 3d XPS in PdCoP-3 positively shifted ca. 0.3 eV compared to that of PdCo ANN. This suggests that the donation of electrons from Pd to P may results in a decrease of the 3d electron density of the Pd atom in PdCoP-3. The result indicates that P atoms in the PdCo alloy modify the electronic structure due to the chemical interactions between Pd, Co and P atoms. This was further demonstrated by the positive shift of Co 2p BE of PdCoP-3 relative to that of PdCo (ESI† Figure S10,). For the case of the P 2p spectrum of PdCoP-3 (Figure 2d), the P 2p peaks at 129.7 and 133.4 eV was assigned to elemental state phosphorus and oxidized phosphorus, which is indicative of PdCoP alloy formation.

Cyclic voltammetry (CVs) was first carried out on PdCoP-3, PdCo ANN and PdCoP GA in N_2 saturated 0.1 mol L^{-1} KOH to evaluate their electrochemical behavior in the absence of N_2H_4 (Figure 3a). All three materials produced a strong oxidation peak from 0.15 to 0.5 V correlating to the oxidation of Co(0) to Co(II) and Co(II) to Co(III). On the reverse sweep, the defined peak near 0.2 V was characteristic of the reduction of Co(II) to Co(0) and Co(III) to Co(II)[8]. The broad and weak peaks at ~ -0.78 V in the forward scan and at ~ -0.45 V in reverse scan were characteristic of Pd oxidation/reduction. The results suggest that both Pd and Co were present in all three catalysts. For PdCoP ANN of the other prepared molar ratios, similar electrochemical behavior was also observed (ESI,† Figure S11).

Journal Name RSCPublishing

ARTICLE

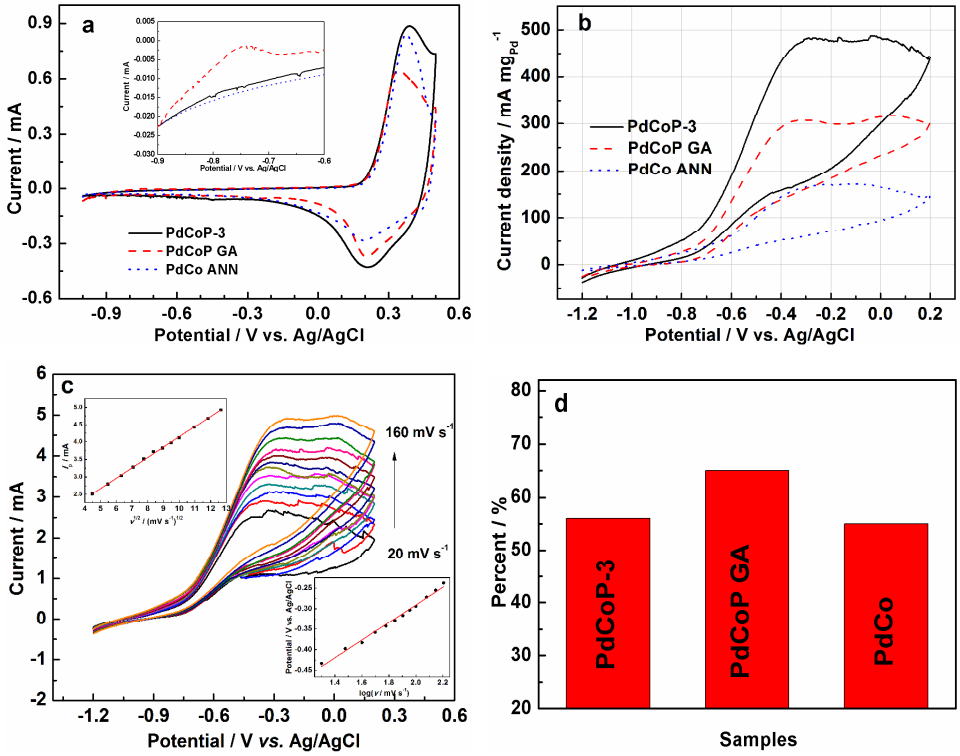

Fig. 3 (a) CVs on PdCoP-3, PdCoP GA and PdCo ANN electrodes in N_2-saturated 0.1 mol L^{-1} KOH solution at a scan rate of 20 mV s^{-1}, the inset shows an enlargement of the forward scan between -0.9 V and -0.6 V. (b) CVs on PdCoP-3, PdCoP GA and PdCo ANN electrodes in N_2-saturated 0.1 mol L^{-1} N_2H_4 + 0.1 mol L^{-1} KOH + 0.1 mol L^{-1} KOH solution at a scan rate of 100 mV s^{-1}. (c) CVs on PdCoP-3 electrode in 0.1 mol L^{-1} N_2H_4 + 0.1 mol L^{-1} KOH + 0.1 mol L^{-1} KOH solution at scan rates of 20, 30, 40, 50, 60, 70, 80, 90, 100, 120, 140 and 160 mV s^{-1} (from bottom to top); the top inset: *Ip vs.* $v^{1/2}$ plot. the bottom inset: *Ep vs.* log(*v*) plot. (d) Percent of the oxidation peak current of the 1000th cycle compared to the initial cycle.

Figure 3b shows CVs of the three catalysts in 0.1 mol L^{-1} N_2H_4 + 0.1 mol L^{-1} KOH +0.1 mol L^{-1} KCl solution. The current was normalized to the Pd mass on the electrodes. In the positive scan direction, the hydrazine onset oxidation potential for the three catalysts was poorly defined by curve slope, thus proving difficult to compare their catalytic activity on this basis. However, the maximum peak current on PdCoP-3, e.g. mass activity, was 483 mA mg^{-1}_{Pd} at ca. -0.30 V, i.e. 1.6 fold that of PdCoP GA (308 mA mg^{-1}_{Pd} at ca. -0.34 V), confirming that the network-like structure was favorable for oxidation of hydrazine. The mass activity on PdCoP-3 was 2.9 times as that of PdCo ANN (168 mA mg^{-1}_{Pd} at ca. -0.28 V), which verified the promotion of P for the catalytic of PdCo alloy. Therefore, both
introduction of P and formation of network structure were beneficial to hydrazine oxidation activity. While introduction of P modified the electron structure of Pd and Co atoms (as demonstrated by XPS analysis), porous network structure favors mass transfer and possibly provides more active sites for catalysis. The effect of Co ratio in PdCoP ANN on catalytic activity for hydrazine oxidation was also investigated (ESI,† Figure S12). Among five catalysts of different Co mass ratio, PdCoP-3 produced the highest catalytic activity for hydrazine oxidation in terms of oxidation peak current density. This indicates that the optimal ratio for highest mass activity was 1:9.2:11 of Pd:Co:P. To further investigate the activity of the all samples, chronoamperrometry measurements were carried out, (Figure S13) (ESI,†). As expected, PdCoP-3 exhibited the highest current density for hydrazine oxidation at 1000 s. This result corresponds well to the CV result. To further evaluate hydrazine oxidation on PdCoP-3, CV was carried out at different scan rates. Figure 3c shows that with increased scan rate, the hydrazine oxidation peak current (*I*p) and peak potential (*E*p) shifted slightly positively. The *I*p increased linearly with the square root of the scan rate ($v^{1/2}$) in the range from 20 to 160 mV s^{-1} (the top inset), indicating the process was influenced by diffusion rather than by surface controlled electron transfer kinetics[28]. Additionally, a linear relationship

between *E*p and log(*v*) was obtained (bottom inset Figure 3c), demonstrating that hydrazine electrooxidation on PdCoP-3 was an irreversible process[29]. We inferred that the overall electro-oxidation of hydrazine (i.e., N_2H_4+ $OH^- \rightarrow N_2 + H_2O + 4e^-$) occurred on PdCoP-3 electrode in alkaline solution. Thus, no peak arose on the negative potential scan in CV test due to the stability of N_2 molecule.

To evaluate the stability of PdCoP-3, PdCoP GA and PdCo ANN, the three samples were subject to accelerated electrochemical degradation tests through repeating potential cycles (ESI,† Figure S14). Decrease in catalytic activity was measured by recording the peak current loss against the cycle number (Figure 3d). After 1000 cycles, the peak current for hydrazine oxidation on PdCoP-3 was ~56% of the initial peak current. While, the peak current on PdCoP GA and PdCo ANN electrodes retained 65% and 55% of the original value respectively, indicating that the stability of PdCoP-3 isn't better than that of PdCoP GA. The degradation of PdCoP-3 may result from the network structure leaching P in alkaline medium[26].

4. Conclusions

PdCoP ANN (alloy nanoparticle network) catalysts were synthesized using a N_2–bubble–template method at room temperature with simultaneous reduction of precursors containing varying ratios of Pd, Co and P. The as-prepared PdCoP ANN had a large BET surface area and mesoporous structure. PdCoP ANN produced higher hydrazine oxidation activity in terms of mass activity than both PdCoP GA (grain aggregates) and PdCo ANN due to its porous structure and the electron donation effect between P and PdCo alloy. Optimal hydrazine oxidation on PdCoP ANN was achieved with a 1:9.2:11 atomic ratio composition of Pd:Co:P. However, PdCoP GA and PdCo ANN appeared to have greater long-term stability than PdCoP ANN, perhaps due to loss of P from the network structure of PdCoP ANN in alkaline media. Overall we conclude that the N_2–bubble–template method, together with varying the molar ratio of reactant precursors, provides a convenient and facile approach to produce alloy catalysts with network structure and high activity.

Acknowledgements

The authors would like to thank the National Natural Science Foundation of China (21363022, 21163018, and 51362027) for financially supporting this work.

Notes and references

[a] College of Chemistry and Chemical Engineering, Northwest Normal University, Lanzhou 730070, China
E-mail: wangrf@nwnu.edu.cn; Fax/Tel: +86 931 7971533
[b] South African Institute for Advanced Materials Chemistry, University of the Western Cape, Private Bag X17, Bellville, Cape Town 7535, South Africa
E-mail: sji@uwc.ac.za; Fax/Tel: +27-21-9599316;

Electronic Supplementary Information (ESI) available: [SEM, XRD, isotherms and electrochemical performance]. See DOI: 10.1039/b000000x/

1. K. Asazawa, K. Yamada, H. Tanaka, A. Oka, M. Taniguchi and T. Kobayashi, *Angew. Chem. Int. Ed.*, 2007, **46**, 8024-8027.
2. C. Roy, E. Bertin, M. H. Martin, S. Garbarino and D. Guay, *Electrocatalysis*, 2013, **4**, 76-84.
3. V. Rosca and M. T. M. Koper, *Electrochim. Acta*, 2008, **53**, 5199-5205.
4. L. Zhang, W. Niu, W. Gao, L. Qi, J. Zhao, M. Xu and G. Xu, *Electrochem. Commun.*, 2013, **37**, 57-60.
5. H. Lin, J. Yang, J. Liu, Y. Huang, J. Xiao and X. Zhang, *Electrochim. Acta*, 2013, **90**, 382-392.
6. M. G. Hosseini, M. M. Momeni and S. Zeynali, *Surf. Eng.*, 2013, **29**, 65-69.
7. Q. Wan, Y. Liu, Z. Wang, W. Wei, B. Li, J. Zou and N. Yang, *Electrochem. Commun.*, 2013, **29**, 29-32.
8. J. Liu, R. Liu, C. L. Yuan, X. P. Wei, J. L. Yin, G. L. Wang and D. X. Cao, *Fuel Cells*, 2013, **5**, 903-909.
9. F. Xu, L. Zhao, F. Zhao, L. Deng, L. Hu and B. Zeng, *Int. J. Electrochem. Sci.*, 2014, **9**, 2832-2847.
10. Q. Hu, G. Li, J. Pan, L. Tan, J. Lu and L. Zhuang, *Int. J. Hydrogen Energy*, 2013, **38**, 16264-16268.
11. Y. Ma, R. Wang, H. Wang, V. Linkov and S. Ji, *Phys. Chem. Chem. Phys.,* 2014, **16**, 3593-3602.
12. J. Yu, Y. Ding, C. Xu, A. Inoue, T. Sakurai and M. Chen, *Chem. Mater.*, 2008, **20**, 4548-4550.
13. W. Wang, R. Wang, H. Wang, S. Ji, J. Key, X. Li and Z. Lei, *J. Power Sources*, 2011, **196**, 9346-9351.
14. W. Wang, S. Ji, H. Wang and R. Wang, *Fuel Cells*, 2012, **12**, 1129-1133.
15. B. C. Tappan, S. A. Steiner and E. P. Luther, *Angew. Chem. Int. Ed.*, 2010, **49**, 4544-4565.
16. Y. Xu, S. Hou, Y. Liu, Y. Zhang, H. Wang and B. Zhang, *Chem. Commun.*, 2012, **48**, 2665-2667.
17. Y. Xu, Y. Yuan, A. Ma, X. Wu, Y. Liu and B. Zhang, *ChemPhysChem,* 2012, **13**, 2601-2609.
18. J. Zhang, Y. Xu and B. Zhang, *Chem. Commun.*, 2014, **50**, 13451-13453.
19. J. Wang, X.-B. Zhang, Z.-L. Wang, L.-M. Wang, W. Xing and X. Liu, *Nanoscale*, 2012, **4**, 1549-1552.
20. A.-K. Herrmann, P. Formanek, L. Borchardt, M. Klose, L. Giebeler, J. Eckert, S. Kaskel, N. Gaponik and A. Eychmüller, *Chem. Mater.*, 2014, **26**, 1074-1083.
21. L. Zhang, D. Lu, Y. Chen, Y. Tang and T. Lu, *J. Mater. Chem. A*, 2014, **2**, 1252-1256.
22. X. Wang, Q. Peng and Y. Li, *Acc. Chem. Res.*, 2007, **40**, 635-643.
23. H. Zhao, C. Yu, H. You, S. Yang, Y. Guo, B. Ding and X. Song, *J. Mater. Chem.,* 2012, **22**, 4780-4789.
24. X. Chen, G. Wu, J. Chen, X. Chen, Z. Xie and X. Wang, *J. Am. Chem. Soc.,* 2011, **133**, 3693-3695.
25. Q. Peng, Y. Dong and Y. Li, *Inorg. Chem.*, 2003, **42**, 2174-2175.
26. R. Wang, Y. Ma, H. Wang, K. Julian and S. Ji, *Chem. Commun.*, 2014, **50**, 12877-12879.
27. A.K. Herrmann, P. Formanek, L. Borchardt, M. Klose, L. Giebeler, J. Eckert, S. Kaskel, N. Gaponik and A. Eychmuller, *Chem. Mater.,* 2014, **26**, 1074-1083.
28. Y. Liang, Y. Zhou, J. Ma, J. Zhao, Y. Chen, Y. Tang and T. Lu, *Appl. Catal. B,* 2011, **103**, 388-396.
29. Y. Liang, K. Wu, C. Ge, Y. Zhou, Y. Chen, Y. Tang and T. Lu, *Fuel Cells*, 2012, **12**, 946-955.

